Atmospheric
Chemistry
and Physics
Discussions

Open Access

1 **Primary and secondary organic aerosol from heated cooking**

2 **oil emissions**

3 Tengyu Liu[1], Zhaoyi Wang[2,3], Xinming Wang[2,4,*], and Chak K. Chan[1,5*]

4 1. School of Energy and Environment, City University of Hong Kong, Hong Kong,

5 China

6 2. State Key Laboratory of Organic Geochemistry and Guangdong Key Laboratory of

7 Environmental Protection and Resources Utilization, Guangzhou Institute of

8 Geochemistry, Chinese Academy of Sciences, Guangzhou, China

9 3. University of Chinese Academy of Sciences, Beijing, China

10 4. Center for Excellence in Urban Atmospheric Environment, Institute of Urban

11 Environment, Chinese Academy of Sciences, Xiamen, China

12 5. City University of Hong Kong Shenzhen Research Institute, Shenzhen, China

13 *Corresponding author:

14 Chak K. Chan

15 School of Energy and Environment, City University of Hong Kong

16 Tel: +852-34425593; Fax: +852-34420688

17 Email: Chak.K.Chan@cityu.edu.hk

18 Xinming Wang

19 State Key Laboratory of Organic Geochemistry

20 Guangzhou Institute of Geochemistry, Chinese Academy of Sciences

21 Tel: +86-20-85290180; Fax: +86-20-85290706

22 Email: wangxm@gig.ac.cn

Atmospheric
Chemistry
and Physics
Discussions

Abstract

23

24 Cooking emissions have been identified as a source of both primary organic aerosol

25 (POA) and secondary organic aerosol (SOA). To examine the characteristics of SOA

26 from cooking emissions, emissions from seven vegetable oils (sunflower, olive, peanut,

27 corn, canola (rapeseed), soybean, and palm oils) heated at 200 °C were photooxidized

28 under high-NO_x conditions in a smog chamber. OA was characterized using a high-

29 resolution time-of-flight aerosol mass spectrometer (HR-TOF-AMS). Sunflower,

30 peanut, corn, canola, and soybean oil generated relatively low concentrations of POA

31 ($\leqslant$ 0.5 µg m^{-3}) in the chamber. For palm and olive oil, positive matrix factorization

32 (PMF) analysis separated POA and SOA better than the residual spectrum method.

33 Temporal trends in concentrations of POA from heated palm oil were accurately

34 predicted assuming first-order POA wall loss. However, this assumption overestimated

35 POA concentrations from heated olive oil, which was attributed to the heterogeneous

36 oxidation of POA. The mass spectra of the PMF resolved POA factor for palm oil, and

37 the average POA from sunflower, peanut, corn, and canola oils were in better agreement

38 (θ = 8–12°) with ambient cooking organic aerosol (COA) factors resolved in select

39 Chinese megacities than those found in given European cities in the literature. The mass

40 spectra of SOA formed from heated cooking oils had high abundances of *m/z*s 27, 28,

41 29, 39, 41, 44, and 55 and displayed limited similarity (θ > 20°) with ambient semi-

42 volatile oxygenated OA (SV-OOA) factors. The entire OA data set measured herein

43 follows a linear trend with a slope of approximately -0.4 in the Van Krevelen diagram,

44 which may indicate oxidation mechanisms involving the addition of both carboxylic

45   acid and alcohol/peroxide functional groups without fragmentation and/or the addition

46   of carboxylic acid functional groups with fragmentation.

Atmospheric
Chemistry
and Physics
Discussions

Open Access

1 Introduction

47

48 Organic aerosol (OA) contributes greatly to atmospheric particulate matter (PM)

49 (Kanakidou et al., 2005), which influences air quality, climate, and human health

50 (Hallquist et al., 2009). OA commonly comprises primary organic aerosol (POA)

51 emitted directly from sources and secondary organic aerosol (SOA) formed via the

52 oxidation of organic gases (Donahue et al., 2009). Cooking is an important source of

53 both POA (Abdullahi et al., 2013) and SOA (Liu et al., 2018). In aerosol mass

54 spectrometer (AMS, Aerodyne Research Incorporated, USA) measurements, cooking

55 OA (COA) has been found to contribute 10–35% of OA in urban areas (Allan et al.,

56 2010; Sun et al., 2011, 2012; Ge et al., 2012; Mohr et al., 2012; Crippa et al., 2013a, b;

57 Xu et al., 2014; Lee et al., 2015), although the AMS may overestimate COA due to the

58 COA relative ionization efficiency (1.56–3.06), which is higher than the typical value

59 of 1.4 used for organics (Reyes-Villegas et al., 2018). In particular, Lee et al. (2015)

60 found that the average contribution of COA to OA (35%) was even higher than that of

61 traffic-related hydrocarbon-like OA (HOA, 26%) at a roadside site in Mongkok in Hong

62 Kong. Xu et al. (2014) also observed higher contributions of COA (24%) than HOA

63 (16%) to OA in Lanzhou, China.

64 Although most of the COA mass spectra resolved by positive matrix factorization

65 (PMF) analysis (Paatero, 1997; Paatero and Tapper, 1994; Ulbrich et al., 2009; Zhang

66 et al., 2011) in the wider AMS dataset have the same basic characteristics, including

67 predominant peaks at m/zs 41, 43, 55, and 57 and high m/z 55/57 ratios, the specific

68 COA mass spectra vary among studies (Mohr et al., 2009; Allan et al., 2010; Sun et al.,

Atmospheric
Chemistry
and Physics
Discussions

69   2011; 2012; Ge et al., 2012; Mohr et al., 2012; Crippa et al., 2013a, b; Lee et al., 2015;

70   Elser et al., 2016; Struchmeier et al., 2016; Aijala et al., 2017). Differing cooking styles

71   may be among the factors that induce this variability in COA mass spectra. For instance,

72   the fraction of *m/z* 41 was higher than that of *m/z* 43 in COA mass spectra for Chinese

73   cooking (He et al., 2010), while the reverse was found for meat cooking (Mohr et al.,

74   2009). Atmospheric aging may also diversify the COA mass spectra. Significantly

75   different COA mass spectra have been resolved during summer and winter in Greece

76   despite the fact that cooking activities are similar during the two seasons (Florou et al.,

77   2017; Kaltsonoudis et al., 2017). In addition, the COA factors resolved by PMF analysis

78   may include emissions from other sources (Dall'Osto et al., 2015) and sometimes

79   cannot be separated from the other factors (Kostenidou et al., 2015; Qin et al., 2017).

80   The multilinear engine (ME-2) is a relatively newly developed tool that can use mass

81   spectra input from the literature to constrain the OA source apportionment solutions

82   (Canonaco et al., 2013). Qin et al. (2017) found that inputting different COA profiles

83   resulted in proportions of COA (to total OA) that differed by factors of up to 2.

84   Comparing laboratory-generated COA mass spectra with ambient PMF factors can help

85   to improve COA source apportionment. Previous studies have been focused on

86   investigating mass spectra of POA from cooking (Mohr et al., 2009; Allan et al., 2010;

87   He et al., 2010; Reyes-Villegas et al., 2018); however, studies exploring mass spectra

88   of SOA from cooking remain scarce.

89   Recent smog chamber studies have demonstrated that cooking emissions can form

90   large amounts of SOA via photochemical aging (Kaltsonoudis et al., 2017; Liu et al.,

Atmospheric
Chemistry
and Physics
Discussions

91   2017, 2018). Kaltsonoudis et al. (2017) observed similarities between aged COA mass

92   spectra from meat charbroiling and corresponding POA mass spectra. Liu et al. (2017)

93   also reported extensive similarities (R^2 of 0.83–0.96) between mass spectra of POA and

94   SOA from heated cooking oils. These mass spectral similarities make it difficult to

95   separate POA and SOA from cooking in smog chamber experiments in terms of both

96   abundance and mass spectral signatures.

97   PMF has been used widely to deconvolve ambient AMS datasets, but relatively

98   less to analyze smog chamber data. Presto et al. (2014) used PMF to analyze POA and

99   SOA from vehicle exhaust. Kaltsonoudis et al. (2017) performed PMF analysis on fresh

100   and aged OA from meat charbroiling. However, PMF analysis has not been applied to

101   POA and SOA from heated cooking oils.

102   Sage et al. (2008) developed a residual spectrum method to separate POA and SOA

103   in diesel exhaust; this residual spectrum method assumes that all signal at m/zs 57 and

104   44 is associated with POA and SOA, respectively. Chirico et al. (2010) and Miracolo et

105   al. (2010) further improved the residual method, using the reduced $C_4H_9^+$ ion as a POA

106   tracer. Chirico et al. (2010) suggested that the appropriate POA tracer ion may differ

107   for different sources. The optimal tracer ions for cooking emissions remain unknown.

108   This study aims to characterize POA and SOA from heated cooking oils emissions,

109   obtain POA and SOA mass spectra via PMF analysis, and compare the resolved mass

110   spectra with those for ambient COA-related factors from PMF. We will also explore the

111   heterogeneous oxidation of POA from palm and olive oils.

112   **2   Materials and methods**

Atmospheric
Chemistry
and Physics
Discussions

2.1 Smog chamber experiments

113

114 Seven photochemical aging experiments were conducted in a 30 m^3 indoor smog

115 chamber at the Guangzhou Institute of Geochemistry, Chinese Academy of Sciences

116 (Wang et al., 2014; Liu et al., 2015, 2016; Deng et al., 2017) (Table 1). The cooking

117 oils tested include sunflower, olive, peanut, corn, canola (rapeseed), soybean, and palm

118 oils, which together constitute over 90% of the vegetable oil consumed globally (USDA,

119 2017). All experiments were conducted at 25 °C and a relative humidity (RH) of less

120 than 5%. Prior to each experiment, the chamber was continuously flushed with purified

121 dry air for at least 48 h. The experimental procedures have been described in detail

122 elsewhere (Liu et al., 2018). Briefly, ammonium sulfate seed particles were introduced

123 first into the chamber to serve as condensation sinks to reduce organic vapor wall losses

124 (Zhang et al., 2014). Then, emissions from heated vegetable oils were introduced into

125 the chamber for 1–1.5 h by an air stream through a 2 m heated (70 °C) Teflon tube. The

126 emissions were generated by heating 250 mL of the target oil at approximately 200 °C

127 in a 500 mL flask in a dimethyl silicone oil bath. Nitrous acid (HONO) was then

128 introduced into the chamber as a source of hydroxyl radical (OH). The initial ratio of

129 non-methane organic gases (NMOGs) to NO_x (NMOG:NO_x) fell largely between 2.6

130 and 5.4 ppbC:ppb, except for the palm oil experiment, in which it was 18.9 ppbC:ppb.

131 These ratios were larger than the typical urban ratio of ~3 (Gordon et al., 2014). After

132 the primary emissions had been characterized for at least 1 h, photochemical aging was

133 initiated by exposing the emissions to black lights (60 W Philips/10R BL365, Royal

134 Dutch Philips Electronics Ltd., the Netherlands) for 2–4.5 h.

135   Gas monitors were used to measure the concentrations of NO_x and O_3 (EC9810,

136   9841T, Ecotech, Australia). NMOGs were characterized using a commercial proton-

137   transfer-reaction time-of-flight mass spectrometer (PTR-TOF-MS, Model 2000, H_3O^+

138   reagent ion, Ionicon Analytik GmbH, Austria) (Lindinger et al., 1998; Jordan et al.,

139   2009). Detailed descriptions of operating conditions, calibrations, and fragmentation

140   corrections can be found elsewhere (Liu et al., 2018). The decay of acrolein or

141   heptadienal was used to determine the OH concentration in the chamber.

142   A scanning mobility particle sizer (SMPS, TSI Incorporated, USA, classifier

143   model 3080, CPC model 3775) was used to measure particle number concentrations

144   and size distributions. The chemical composition of submicron non-refractory

145   particulate matter (NR-PM$_1$) was characterized using a high-resolution time-of-flight

146   aerosol mass spectrometer (hereafter AMS, Aerodyne Research Incorporated, USA)

147   (DeCarlo et al., 2006). The instrument alternated between the high-sensitivity V-mode

148   and the high-resolution W-mode every 1 min. The Squirrel 1.57I and Pika 1.16I toolkits

149   were used in IGOR (Wavemetrics Inc., USA) to analyze the AMS data; the Aiken et al.

150   (2008) fragmentation table was adopted. Elemental ratios, such as the hydrogen-to-

151   carbon ratio (H:C) and oxygen-to-carbon ratio (O:C), were determined using the

152   improved-ambient method (Canagaratna et al., 2015). HEPA-filtered particle-free air

153   from the chamber was measured for at least 20 min before and after each experiment to

154   determine the major gas signals. The ionization efficiency was calibrated using 300 nm

155   ammonium nitrate particles.

156   **2.2 Separating POA and SOA**

Atmospheric
Chemistry
and Physics
Discussions

157   The experiments in this study were classified into two groups (Table 1). Sunflower,

158   peanut, corn, canola, and soybean oil emissions produced low POA concentrations (<

159   0.5 µg m^{-3}) in the smog chamber. Due to wall losses, the POA concentration was close

160   to the AMS detection limit when the lights were turned on (e.g., the sunflower oil

161   experiment in Supplementary Fig. S1). These experiments were therefore assumed to

162   involve only SOA. POA and SOA mixtures were present in the palm and olive oil

163   experiments, which produced maximum POA concentrations of 14 and 39 µg m^{-3},

164   respectively. PMF analysis (Paatero, 1997; Paatero and Tapper, 1994) was performed

165   on the high-resolution mass spectra (*m/z*s 12–160) to deconvolve the POA and SOA

166   factors following the procedure of Ulbrich et al. (2009). PMF solutions were examined

167   for 1 to 5 factors with fPeak values varying from -1 to 1. Diagnostic plots are shown

168   for all datasets in Figs. S2 and S3. After examining the PMF residuals, time series for

169   different numbers of factors, and mass spectral similarity between PMF POA and

170   observed POA spectra, 2-factor solutions with fPeak values of -0.2 and 0 were chosen

171   for the palm and olive oil experiments, respectively.

172   The residual spectrum method (Sage et al., 2008; Chirico et al., 2010; Miracolo et

173   al., 2010; Presto et al., 2014) was used in addition to PMF analysis to separate the POA

174   and SOA. The residual method assumes that all tracer ion signal (e.g., $C_4H_9^+$) is

175   associated with POA and that the chemical composition of POA remains constant

176   throughout the entire experiment. The mass concentration of POA at time *t* can then be

177   calculated using the following equation:

178                           $$POA_t = Ion_t / Ion_{t_0} \times OM_{t_0}, \qquad (1)$$

Atmospheric
Chemistry
and Physics
Discussions

Open Access
EGU

179   where OM_{t0} is the total organic matter concentration at time $t = 0$, and Ion_t and Ion_{t0} are

180   the organic mass signals of a specific POA tracer ion at time t and time $t = 0$ (lights on),

181   respectively. $C_4H_9^+$ is typically chosen as the POA tracer for combustion sources (Sage

182   et al., 2008; Chirico et al., 2010; Miracolo et al., 2010; Presto et al., 2014); the optimal

183   tracer ion for cooking emissions remain unclear. The tracer ions tested in this study

184   include $C_4H_7^+$, $C_4H_9^+$, $C_5H_8^+$, $C_5H_9^+$, $C_6H_9^+$, and $C_7H_9^+$.

3   Results and discussion

3.1 POA-SOA split

187   Figure 1 shows measured OA time series for the palm and olive oil experiments; the

188   OA concentrations were not corrected for particle wall loss. The experiments typically

189   involved introduction of the cooking emissions to the chamber (~1–1.5 h),

190   characterization of primary emissions (~1–2 h), and photochemical aging (2–4.5 h). In

191   the palm oil experiment, the POA concentration increased rapidly during the first ~1.6

192   h of the emission introduction period, reaching approximately 14 µg m^{-3}. The POA

193   concentration then decreased to ~9 µg m^{-3} due to wall losses. SOA was quickly formed

194   after photochemical aging was initiated at $t = 0$, and the OA concentration increased by

195   a factor of 5 in less than 1 h. The maximum POA concentration in the olive oil

196   experiment was approximately two times higher than that in the palm oil experiment,

197   and the maximum OA concentration was ~50% of that in the palm oil experiment via

198   SOA formation. Palm oil produced SOA more efficiently than did olive oil; this is

199   consistent with our previous study, which found that the SOA production rate of palm

200   oil was 4 times that of olive oil, likely due to the higher abundance of SOA precursors

Atmospheric
Chemistry
and Physics
Discussions

201   in palm oil emissions (Liu et al., 2018).

202   Figure 1 also shows time series of measured OA, resolved PMF factors, and POA

203   concentrations assuming first-order loss of POA to the walls. Two factors, namely POA

204   and SOA, were identified. Solutions with three or more factors introduced physically

205   inexplicable factors and did not improve the PMF performance (Fig. S4). Overall, the

206   OA reconstructed by PMF accurately captured the trends in measured OA throughout

207   the experiment. The sum of the residual was generally less than 2 µg m^{-3}, resulting in

208   ratios of total residual concentration (ΣResidual) to total OA concentration (ΣOA) of

209   less than 5% (Figs. S2 and S3). The separation of POA and SOA factors was reasonable

210   and interpretable. During the introduction and characterization of cooking emissions (t

211   < 0), the concentrations of SOA should be, by definition, exactly zero. The

212   concentrations of the resolved SOA factors were approximately 0.3 µg m^{-3}, capturing

213   the expected behavior.

214   In previous smog chamber studies of dilute emissions from combustion sources

215   (Weitkamp et al., 2007; Gordon et al., 2014; Liu et al., 2015, 2016), POA was typically

216   assumed to be inert, and POA concentrations followed first-order wall loss equations.

217   Figure 1 shows POA concentrations after the onset of photooxidation assuming first-

218   order wall loss. The wall loss rate constants were determined from the decay of POA

219   during the primary emissions characterization period. For palm oil, the predicted POA

220   concentrations agreed well with the PMF POA factor, suggesting that the assumption

221   of POA inertness was reasonable. However, for olive oil, the concentration of the PMF

222   POA factor was significantly lower after the onset of photooxidation (t = 0) than the

Atmospheric
Chemistry
and Physics
Discussions

223   POA concentration predicted assuming first-order wall losses. The PMF POA factor

224   decreased rapidly in the first hour after $t = 0$, which may have been due to the

225   heterogeneous oxidation of POA. Kaltsonoudis et al. (2016) observed similar changes

226   in POA concentrations when emissions from meat charbroiling were exposed to OH

227   levels similar to those used in this experiment. Nah et al. (2013) also observed rapid

228   heterogeneous OH oxidation of select cooking POA components such as oleic acid and

229   linoleic acid. The differences in POA behavior may have arisen from the different

230   chemical compositions, and corresponding differences in reactivity, of POA from olive

231   and palm oils.

232   To validate the differences in heterogeneous oxidation reactivity between POA

233   from palm and olive oils, two additional ozonolysis experiments were conducted

234   separately using an oxidation flow reactor. Emissions generated in the flask were first

235   passed continuously through the reactor for at least 30 min and then exposed to 500–

236   600 ppb of ozone (O_3) for another 17 min. The total flow rate and residence time in the

237   flow reactor were 6 L min^{-1} and 75 s, respectively. OH radicals were not present in these

238   experiments. Previous work has demonstrated that exposing gas-phase emissions from

239   heated cooking oils to O_3 does not lead to SOA formation (Liu et al., 2017). Therefore,

240   any changes in OA chemical composition during these ozonolysis experiments were

241   attributed to heterogeneous oxidation. Figure 2 shows time series of O:C ratios and O_3

242   concentrations during the ozonolysis experiments. The olive oil O:C ratio increased

243   from 0.11 to 0.17 after the emissions were exposed to O_3 for 17 min; no obvious

244   changes were observed in the palm oil O:C ratio. These results demonstrate that POA

Atmospheric
Chemistry
and Physics
Discussions

Open Access

245   from olive oil undergoes heterogeneous ozone oxidation more readily than POA from

246   palm oil. The olive oil POA may contain more abundant unsaturated organic species,

247   which are expected to react quickly with OH radicals (Atkinson and Arey, 2003).

248   Figure 3 shows POA concentrations obtained using the residual method with

249   different POA tracer ions, along with the PMF-derived POA factors. For the palm oil

250   experiment, the residual method overestimated the POA concentrations (compared with

251   PMF) using all of the different tracer ions. For the olive oil experiment, the residual

252   method accurately predicted the POA concentrations before the lights were turned on

253   using different tracer ions. However, after photochemical aging began, the residual

254   method did not agree with the PMF results. Using $C_5H_9^+$ as a POA tracer, the residual

255   method captured the changes in POA during the first 1 h, but overestimated the POA

256   concentrations by as much as a factor of 2 for the remainder of the experiment; use of

257   the other ions led to significant POA concentration overestimation in comparison with

258   the PMF-resolved POA concentrations. The POA concentrations determined using

259    $C_4H_7^+$, $C_4H_9^+$, and $C_7H_9^+$ were higher even than those estimated for first-order POA

260   loss; this may be attributed to the presence of these ions in SOA, which is then

261   incorrectly allocated to POA by the residual method. These observations indicate that

262   the use of associated tracer ions to calculate POA is not valid for the photochemical

263   aging of cooking oil emissions.

264   Overall, PMF analysis effectively separated POA and SOA from heated cooking

265   oils. The traditional method, which assumes first-order POA wall loss, worked well

266   when the POA was inert, as in the palm oil experiment, but greatly overestimated the

Atmospheric
Chemistry
and Physics
Discussions

Open Access

EGU

267   POA concentration in the olive oil experiment, which was attributed to the occurrence

268   of heterogeneous oxidation. The residual method failed to capture the POA

269   concentrations using any of the different POA tracer ions due to the presence of these

270   ions in the SOA mass spectrum.

271   **3.2 Mass spectra of PMF-resolved factors**

272   Figure 4 shows mass spectra of POA emissions and PMF-derived POA factors from the

273   olive and palm oils. These were also compared to the average mass spectrum of POA

274   emitted from heated sunflower, peanut, corn, and canola oils obtained from Liu et al.

275   (2017). Overall, for both oils, the POA factor mass spectra agreed very well with the

276   directly measured POA spectra. For both oil types, the θ angles between the factor and

277   measured mass spectra were less than 5°; generally, θ angles of 0–5°, 5–10°, 10–15°,

278   15–30°, and > 30° indicate excellent agreement, good agreement, many similarities,

279   limited similarities, and poor agreement, respectively, between two mass spectra

280   (Kostenidou et al., 2009; Kaltsonoudis et al., 2017). The PMF analysis slightly

281   underestimated the mass fraction at m/z 28 and slightly overestimated the mass fractions

282   at m/zs 41 and 55 in both experiments.

283   The olive oil POA factor was dominated by m/z 41 (f_{41} = 0.105), followed by m/zs

284   69 (f_{69} = 0.088), 55 (f_{55} = 0.075), and 43 (f_{43} = 0.050). In the high-resolution mass

285   spectra, the most abundant ions in these unit masses were $C_3H_5^+$, $C_5H_9^+$, $C_4H_7^+$, and

286    $C_3H_7^+$, respectively (Fig. S5). The olive oil POA factor mass spectrum showed limited

287   similarity (θ = 26°) to the average POA mass spectrum for the other cooking oils. The

288   m/z 69 abundance in the POA factor was significantly higher than those (average f_{69} =

Atmospheric
Chemistry
and Physics
Discussions

289   0.026) in POA from other oils, while the mass fractions of *m/z*s 29, 43, and 55 were

290   generally lower. The mass spectrum of olive oil POA measured directly in this study

291   also exhibited poor agreement ($\theta = 31°$) with olive oil POA mass spectra measured in

292   an oxidation flow reactor (Liu et al., 2017) (Fig. S6). The mass spectral differences

293   between this study and Liu et al. (2017) may have arisen from the different oil heating

294   temperatures and dilution conditions.

295   The palm oil POA factor was dominated by *m/z* 55 ($f_{55} = 0.092$), followed by *m/z*s

296   41 ($f_{41} = 0.089$) and 43 ($f_{43} = 0.069$); the most abundant ions in these unit masses were

297    $C_4H_7^+$, $C_3H_5^+$, and $C_3H_7^+$, respectively (Fig. S5). The high abundances of *m/z*s 41 and

298   55 are similar to previous studies showing POA emissions from heated peanut, canola,

299   and sunflower oils (Allan et al., 2010), Chinese cooking (He et al., 2010), and meat

300   charbroiling (Kaltsonoudis et al., 2017). The POA factor mass spectrum exhibited good

301   agreement ($\theta = 9°$) with the average mass spectrum of POA from other cooking oils,

302   although the POA factor had relatively higher mass fractions of *m/z*s 67 and 69 and

303   lower abundances of *m/z*s 28 and 29. The palm oil POA factor had higher abundances

304   of oxygen-containing ions such as CO^+, CHO^+, CO_2^+, and $C_3H_3O^+$ than did the olive

305   oil POA factor, resulting in a relatively higher O:C ratio (palm O:C = 0.15; olive O:C

306   = 0.09).

307   Figure 5 shows PMF-derived SOA factor mass spectra of palm and olive oil and

308   the average mass spectrum of SOA formed from sunflower, peanut, corn, canola, and

309   soybean oils, which was obtained over a 10 min period after the OA concentration

310   reached its maximum for each oil. The SOA factors were dominated by *m/z*s 27, 28, 29,

Atmospheric
Chemistry
and Physics
Discussions

311   41, 43, 44, and 55; the most abundant ions in these unit masses were $C_2H_3^+$, CO^+, CHO^+,

312    $C_3H_5^+$, $C_2H_3O^+$, CO_2^+, and $C_4H_7^+$, respectively (Fig. S5). The abundances of oxygen-

313   containing ions were generally higher than those in the corresponding POA factors. The

314   mass fraction at m/z 43 (f_{43} = 0.087) was higher than f_{44} (0.059) in the olive oil SOA

315   factor, while f_{44} (0.074) dominated f_{43} (0.067) in the palm oil SOA factor. Despite these

316   differences, the mass spectra of the two SOA factors exhibited good agreement ($\theta = 8°$).

317   Although the olive oil and palm oil had different NMOG compositions (Liu et al., 2018)

318   and POA mass spectra, the SOA produced by the two oils had highly similar mass

319   spectra. The SOA factor mass spectra were also highly similar ($\theta = 15°$ for olive oil, 7°

320   for palm oil) to the average mass spectrum of SOA from five other cooking oils, which

321   contained a higher mass fraction of m/z 44 (average f_{44} = 0.080). $C_4H_7^+$, $C_4H_9^+$, $C_5H_8^+$,

322    $C_5H_9^+$, $C_6H_9^+$, and $C_7H_9^+$ ions were present in both SOA factors, which led to the

323   incorrect separation of the POA and SOA by the residual method, as discussed above.

324   **3.3 Comparison of PMF-resolved factors with ambient factors**

325   Comparisons of mass spectra from laboratory-generated cooking OA with ambient

326   PMF-resolved COA factors can help to constrain COA source apportionment. Figure

327   6a summarizes θ angles between ambient COA factors from other studies and the palm

328   oil PMF POA spectrum, average PMF SOA spectrum, and average POA and SOA

329   spectra from cooking oils. The olive oil POA mass spectrum was not included in the

330   comparison as it can vary greatly under different experimental conditions. The

331   reference mass spectra from other studies were obtained from the AMS spectral

332   database (Ulbrich, I.M., Handschy, A., Lechner, M., and Jimenez, J.L., High-Resolution

333   AMS Spectral Database. URL: http://cires.colorado.edu/jimenez-group/HRAMSsd/)

334   (Ulbrich et al., 2009). The agreement between ambient COA factors and the palm PMF

335   POA and average POA mass spectra decreased from 8–12° for ambient COA factors

336   from the commercial and shopping area of Mongkok in Hong Kong (Lee et al., 2015)

337   to 25–28° for ambient COA factors from a suburban area in Pasadena (Hayes et al.,

338   2013). Cooking style may be among the factors that drives this variability in θ. Mass

339   spectral agreement was better for urban areas in Hong Kong, Beijing, and Xi'an, where

340   stir-frying foods with vegetable oils is popular, than in urban European cities, where

341   grilling and broiling are prevalent (Abdullahi et al., 2013). Atmospheric oxidation may

342   also influence the correlations between the POA factor mass spectra found herein and

343   the ambient COA factors. For example, the mass spectrum of a cooking-influenced

344   organic aerosol (CIOA) factor identified in Pasadena (Hayes et al., 2013) displayed

345   better agreement with the SOA factor and average SOA mass spectra than with the POA

346   factor and average POA spectra. Kaltsonoudis et al. (2017) also found that this CIOA

347   factor correlated well with mass spectra of aged OA from meat charbroiling. The

348   average PMF SOA factor and average SOA spectrum derived herein were poorly

349   correlated (θ generally > 30°) with other ambient COA factors (Mohr et al., 2009;

350   Crippa et al., 2013a, b; Lee et al., 2015; Elser et al., 2016; Struchmeier et al., 2016;

351   Aijala et al., 2017). Our results suggest that one should consider the cooking style and

352   atmospheric oxidation conditions when constraining COA factors with the default COA

353   mass spectral inputs.

354   Figure 7 compares the average PMF SOA factor mass spectrum and average

355   ambient semi-volatile oxygenated organic aerosol (SV-OOA) factor (Ng et al., 2011a).

356   SV-OOA is ubiquitous in the atmosphere and generally associated with SOA (Ng et al.,

357   2010). The SV-OOA factor mass spectrum was recalculated following the Aiken et al.

358   (2008) fragmentation table, assuming that the OA mass at m/z 28 was equal to that at

359   m/z 44 and that m/z 18 was equal to 22.5% of m/z 44. The average mass spectrum of

360   the PMF SOA factors exhibited poor agreement with the SV-OOA average mass

361   spectrum ($\theta = 25°$). The average PMF SOA factor for cooking oils had higher

362   abundances of m/zs 27, 28, 29, 39, 41, 44, and 55 than did the SV-OOA factor and lower

363   mass fractions of m/zs 15 and 43. In particular, the SV-OOA spectrum had no signal at

364   m/z 39, while the PMF SOA factor f_{39} was 0.048. The average mass spectra of the PMF

365   SOA factors and SOA from other cooking oils were also unlike other ambient SV-OOA

366   factors ($\theta > 20°$) (Mohr et al., 2009; Crippa et al., 2013a; Hayes et al., 2013;

367   Struchmeier et al., 2016; Aijala et al., 2017) (Fig. 6b). The poor correlations between

368   cooking SOA and SV-OOA were not unexpected, as ambient SV-OOA may contain a

369   mixture of SOA from numerous sources, such as vehicle exhaust, biomass burning, and

370   industrial and biogenic emissions.

371   **3.4 OA oxidation state and chemical evolution**

372   Figure 8 shows the H:C and O:C ratios of PMF-resolved POA and SOA factors, SOA

373   from heated cooking oils, and ambient COA and SV-OOA factors in a Van Krevelen

374   diagram. The O:C ratio and estimated average carbon oxidation state (OS_C) ($OS_C \approx$

375    $2 \times$ O:C $-$ H:C) (Kroll et al., 2011) generally increase with increasing atmospheric

Atmospheric
Chemistry
and Physics
Discussions

376   OA aging. The O:C ratios for the olive and palm PMF POA were 0.09 and 0.15,

377   respectively, comparable to those found for Chinese cooking (0.08–0.13) and meat

378   charbroiling (0.10) (Kaltsonoudis et al., 2017). The O:C ratios for the olive and palm

379   PMF SOA and SOA from other cooking oils ranged from 0.40 to 0.50, slightly lower

380   than that of SV-OOA (0.53), which indicates that the SOA formed from cooking oils

381   herein was less oxidized than ambient SV-OOA. In Van Krevelen space, the entire

382   dataset features a linear trend with a slope of approximately -0.4, which may indicate

383   oxidation mechanisms involving the addition of both carboxylic acid and

384   alcohol/peroxide functional groups without fragmentation and/or the addition of

385   carboxylic acid functional groups with fragmentation (Heald et al., 2010; Ng et al.,

386   2011b). This slope is consistent with the aging of ambient OOA (Ng et al., 2011b) and

387   lower than the -0.8 slope noted in evolving ambient OA data corrected using the

388   improved-ambient method (Heald et al., 2010). The O:C ratios of these ambient COA

389   factors ranged from 0.11 to 0.34, consistent with the oxidation trends determined for

390   cooking OA in this study. Some of the COA factors had O:C ratios higher than those

391   noted for POA from cooking emissions in laboratory studies (e.g., O:C = 0.27 for CIOA

392   in Pasadena (Hayes et al., 2013) and O:C = 0.34 for COA in Atlanta (Xu et al., 2018));

393   it is possible that these COA factors contained aged OA and/or SOA formed from

394   cooking emissions.

395   **4   Conclusions**

396   SOA formation from heated cooking oil emissions was investigated in a smog chamber

397   under high-NO$_x$ conditions. For experiments with mixtures of POA and SOA, the POA

Atmospheric
Chemistry
and Physics
Discussions

398   and SOA factors were separated using PMF, the traditional method, and the residual

399   method; PMF outperformed the other techniques in resolving accurate POA and SOA

400   factors. Although the traditional method, which assumes first-order POA wall losses,

401   worked well when the POA was inert, it greatly overestimated the POA concentration

402   when heterogeneous oxidation occurred. The residual method, which uses different ions

403   as POA tracers, failed to capture the POA concentrations due to the presence of these

404   ions in the SOA mass spectrum.

405   Mass spectra of palm oil PMF POA and average POA from other cooking oils

406   exhibited good agreement ($\theta = 8$–$14°$) with ambient COA factors resolved in select

407   Chinese megacities such as Hong Kong, Beijing, and Xi'an and less similarity ($\theta = 11$–

408    $23°$) with ambient COA factors determined in select European cities. The mass

409   spectrum of a CIOA factor determined in Pasadena was more consistent with the

410   average PMF SOA factor mass spectrum ($\theta = 17°$) than with the POA factors ($\theta = 25$–

411    $28°$). Our results suggest that one should consider the cooking style and atmospheric

412   oxidation conditions when performing deconvolution analyses with the default COA

413   mass spectral inputs.

414   The average mass spectra of PMF SOA factors and SOA from other cooking oils

415   exhibited little similarity ($\theta > 20°$) to ambient SV-OOA factors, which is not unexpected

416   given that SV-OOA may contain a mixture of SOA from many sources. In the Van

417   Krevelen diagram, the entire data set in this study yielded a linear trend with a slope of

418   approximately -0.4, which may indicate oxidation mechanisms involving the addition

Atmospheric
Chemistry
and Physics
Discussions

Open Access

419   of both carboxylic acid and alcohol/peroxide functional groups without fragmentation

420   and/or the addition of carboxylic acid functional groups with fragmentation.

Atmospheric
Chemistry
and Physics
Discussions

References

427   Abdullahi, K. L., Delgado-Saborit, J. M., and Harrison, R. M.: Emissions and indoor
428   concentrations of particulate matter and its specific chemical components from
429   cooking: A review, Atmos. Environ., 71, 260-294,
430   https://doi.org/10.1016/j.atmosenv.2013.01.061, 2013.
431   Äijälä, M., Heikkinen, L., Fröhlich, R., Canonaco, F., Prévôt, A. S. H., Junninen, H., Petäjä,
432   T., Kulmala, M., Worsnop, D., and Ehn, M.: Resolving anthropogenic aerosol
433   pollution types – deconvolution and exploratory classification of pollution events,
434   Atmos. Chem. Phys., 17, 3165-3197, https://doi.org/10.5194/acp-17-3165-2017,
435   2017.
436   Aiken, A. C., DeCarlo, P. F., Kroll, J. H., Worsnop, D. R., Huffman, J. A., Docherty, K. S.,
437   Ulbrich, I. M., Mohr, C., Kimmel, J. R., Sueper, D., Sun, Y., Zhang, Q., Trimborn,
438   A., Northway, M., Ziemann, P. J., Canagaratna, M. R., Onasch, T. B., Alfarra, M. R.,
439   Prevot, A. S. H., Dommen, J., Duplissy, J., Metzger, A., Baltensperger, U., and
440   Jimenez, J. L.: O/C and OM/OC Ratios of Primary, Secondary, and Ambient Organic
441   Aerosols with High-Resolution Time-of-Flight Aerosol Mass Spectrometry, Environ.
442   Sci. Technol., 42, 4478-4485, 10.1021/es703009q, 2008.
443   Allan, J. D., Williams, P. I., Morgan, W. T., Martin, C. L., Flynn, M. J., Lee, J., Nemitz, E.,
444   Phillips, G. J., Gallagher, M. W., and Coe, H.: Contributions from transport, solid
445   fuel burning and cooking to primary organic aerosols in two UK cities, Atmos. Chem.
446   Phys., 10, 647-668, https://doi.org/10.5194/acp-10-647-2010, 2010.
447   Atkinson, R., and Arey, J.: Atmospheric Degradation of Volatile Organic Compounds, Chem.
448   Rev., 103, 4605-4638, https://doi.org/10.1021/cr0206420, 2003.
449   Canagaratna, M. R., Jimenez, J. L., Kroll, J. H., Chen, Q., Kessler, S. H., Massoli, P.,
450   Hildebrandt Ruiz, L., Fortner, E., Williams, L. R., Wilson, K. R., Surratt, J. D.,
451   Donahue, N. M., Jayne, J. T., and Worsnop, D. R.: Elemental ratio measurements of
452   organic compounds using aerosol mass spectrometry: characterization, improved
453   calibration, and implications, Atmos. Chem. Phys., 15, 253-272,
454   https://doi.org/10.5194/acp-15-253-2015, 2015.
455   Canonaco, F., Crippa, M., Slowik, J. G., Baltensperger, U., and Prévôt, A. S. H.: SoFi, an
456   IGOR-based interface for the efficient use of the generalized multilinear engine (ME-
457   2) for the source apportionment: ME-2 application to aerosol mass spectrometer data,
458   Atmos. Meas. Tech., 6, 3649-3661, https://doi.org/10.5194/amt-6-3649-2013, 2013.
459   Chirico, R., DeCarlo, P. F., Heringa, M. F., Tritscher, T., Richter, R., Prévôt, A. S. H.,
460   Dommen, J., Weingartner, E., Wehrle, G., Gysel, M., Laborde, M., and
461   Baltensperger, U.: Impact of aftertreatment devices on primary emissions and
462   secondary organic aerosol formation potential from in-use diesel vehicles: results
463   from smog chamber experiments, Atmos. Chem. Phys., 10, 11545-11563,
464   https://doi.org/10.5194/acp-10-11545-2010, 2010.
465   Crippa, M., DeCarlo, P. F., Slowik, J. G., Mohr, C., Heringa, M. F., Chirico, R., Poulain, L.,
466   Freutel, F., Sciare, J., Cozic, J., Di Marco, C. F., Elsasser, M., Nicolas, J. B.,
467   Marchand, N., Abidi, E., Wiedensohler, A., Drewnick, F., Schneider, J., Borrmann,
468   S., Nemitz, E., Zimmermann, R., Jaffrezo, J. L., Prévôt, A. S. H., and Baltensperger,

Atmospheric
Chemistry
and Physics
Discussions

469 U.: Wintertime aerosol chemical composition and source apportionment of the

470 organic fraction in the metropolitan area of Paris, Atmos. Chem. Phys., 13, 961-981,

471 https://doi.org/10.5194/acp-13-961-2013, 2013a.

472 Crippa, M., El Haddad, I., Slowik, J. G., DeCarlo, P. F., Mohr, C., Heringa, M. F., Chirico,

473 R., Marchand, N., Sciare, J., Baltensperger, U., and Prévôt, A. S. H.: Identification of

474 marine and continental aerosol sources in Paris using high resolution aerosol mass

475 spectrometry, J. Geophys. Res.-Atmos., 118, 1950-1963,

476 https://doi.org/10.1002/jgrd.50151, 2013b.

477 Dall'Osto, M., Paglione, M., Decesari, S., Facchini, M. C., O'Dowd, C., Plass-Duellmer, C.,

478 and Harrison, R. M.: On the Origin of AMS "Cooking Organic Aerosol" at a Rural

479 Site, Environ. Sci. Technol., 49, 13964-13972,

480 https://doi.org/10.1021/acs.est.5b02922, 2015.

481 DeCarlo, P. F., Kimmel, J. R., Trimborn, A., Northway, M. J., Jayne, J. T., Aiken, A. C.,

482 Gonin, M., Fuhrer, K., Horvath, T., Docherty, K. S., Worsnop, D. R., and Jimenez, J.

483 L.: Field-Deployable, High-Resolution, Time-of-Flight Aerosol Mass Spectrometer,

484 Anal. Chem., 78, 8281-8289, https://doi.org/10.1021/ac061249n, 2006.

485 Deng, W., Hu, Q., Liu, T., Wang, X., Zhang, Y., Song, W., Sun, Y., Bi, X., Yu, J., Yang, W.,

486 Huang, X., Zhang, Z., Huang, Z., He, Q., Mellouki, A., and George, C.: Primary

487 particulate emissions and secondary organic aerosol (SOA) formation from idling

488 diesel vehicle exhaust in China, Sci. Total Environ., 593–594, 462-469,

489 https://doi.org/10.1016/j.scitotenv.2017.03.088, 2017.

490 Elser, M., Huang, R. J., Wolf, R., Slowik, J. G., Wang, Q., Canonaco, F., Li, G., Bozzetti, C.,

491 Daellenbach, K. R., Huang, Y., Zhang, R., Li, Z., Cao, J., Baltensperger, U., El-

492 Haddad, I., and Prévôt, A. S. H.: New insights into PM2.5 chemical composition and

493 sources in two major cities in China during extreme haze events using aerosol mass

494 spectrometry, Atmos. Chem. Phys., 16, 3207-3225, https://doi.org/10.5194/acp-16-

495 3207-2016, 2016.

496 Florou, K., Papanastasiou, D. K., Pikridas, M., Kaltsonoudis, C., Louvaris, E., Gkatzelis, E.,

497 Patoulias, D., Mihalopoulos, N., and Pandis, S. N.: The contribution of wood burning

498 and other pollution sources to wintertime organic aerosol levels in two Greek cities,

499 Atmos. Chem. Phys., 17, 3145-3163, https://doi.org/10.5194/acp-17-3145-2017,

500 2017.

501 Ge, X., Setyan, A., Sun, Y., and Zhang, Q.: Primary and secondary organic aerosols in

502 Fresno, California during wintertime: Results from high resolution aerosol mass

503 spectrometry, J. Geophys. Res.-Atmos., 117, D19301,

504 https://doi.org/10.1029/2012JD018026, 2012.

505 Gordon, T. D., Presto, A. A., May, A. A., Nguyen, N. T., Lipsky, E. M., Donahue, N. M.,

506 Gutierrez, A., Zhang, M., Maddox, C., Rieger, P., Chattopadhyay, S., Maldonado, H.,

507 Maricq, M. M., and Robinson, A. L.: Secondary organic aerosol formation exceeds

508 primary particulate matter emissions for light-duty gasoline vehicles, Atmos. Chem.

509 Phys., 14, 4661-4678, https://doi.org/10.5194/acp-14-4661-2014, 2014.

510 Hallquist, M., Wenger, J. C., Baltensperger, U., Rudich, Y., Simpson, D., Claeys, M.,

511 Dommen, J., Donahue, N. M., George, C., Goldstein, A. H., Hamilton, J. F.,

512 Herrmann, H., Hoffmann, T., Iinuma, Y., Jang, M., Jenkin, M. E., Jimenez, J. L.,

513   Kiendler-Scharr, A., Maenhaut, W., McFiggans, G., Mentel, T. F., Monod, A.,
514   Prévôt, A. S. H., Seinfeld, J. H., Surratt, J. D., Szmigielski, R., and Wildt, J.: The
515   formation, properties and impact of secondary organic aerosol: current and emerging
516   issues, Atmos. Chem. Phys., 9, 5155-5236, https://doi.org/10.5194/acp-9-5155-2009,
517   2009.
518 Hayes, P. L., Carlton, A. G., Baker, K. R., Ahmadov, R., Washenfelder, R. A., Alvarez, S.,
519   Rappenglück, B., Gilman, J. B., Kuster, W. C., de Gouw, J. A., Zotter, P., Prévôt, A.
520   S. H., Szidat, S., Kleindienst, T. E., Offenberg, J. H., Ma, P. K., and Jimenez, J. L.:
521   Modeling the formation and aging of secondary organic aerosols in Los Angeles
522   during CalNex 2010, Atmos. Chem. Phys., 15, 5773-5801,
523   https://doi.org/10.5194/acp-15-5773-2015, 2015.
524 He, L. Y., Lin, Y., Huang, X. F., Guo, S., Xue, L., Su, Q., Hu, M., Luan, S. J., and Zhang, Y.
525   H.: Characterization of high-resolution aerosol mass spectra of primary organic
526   aerosol emissions from Chinese cooking and biomass burning, Atmos. Chem. Phys.,
527   10, 11535-11543, https://doi.org/10.5194/acp-10-11535-2010, 2010.
528 Heald, C. L., Kroll, J. H., Jimenez, J. L., Docherty, K. S., DeCarlo, P. F., Aiken, A. C., Chen,
529   Q., Martin, S. T., Farmer, D. K., and Artaxo, P.: A simplified description of the
530   evolution of organic aerosol composition in the atmosphere, Geophys. Res. Lett., 37,
531   L08803, https://doi.org/10.1029/2010gl042737, 2010.
532 Jordan, A., Haidacher, S., Hanel, G., Hartungen, E., Mark, L., Seehauser, H., Schottkowsky,
533   R., Sulzer, P., and Mark, T. D.: A high resolution and high sensitivity proton-transfer-
534   reaction time-of-flight mass spectrometer (PTR-TOF-MS), Int. J. Mass Spectrom.,
535   286, 122-128, 2009.
536 Kaltsonoudis, C., Kostenidou, E., Louvaris, E., Psichoudaki, M., Tsiligiannis, E., Florou, K.,
537   Liangou, A., and Pandis, S. N.: Characterization of fresh and aged organic aerosol
538   emissions from meat charbroiling, Atmos. Chem. Phys., 17, 7143-7155,
539   https://doi.org/10.5194/acp-17-7143-2017, 2017.
540 Kanakidou, M., Seinfeld, J. H., Pandis, S. N., Barnes, I., Dentener, F. J., Facchini, M. C., Van
541   Dingenen, R., Ervens, B., Nenes, A., Nielsen, C. J., Swietlicki, E., Putaud, J. P.,
542   Balkanski, Y., Fuzzi, S., Horth, J., Moortgat, G. K., Winterhalter, R., Myhre, C. E. L.,
543   Tsigaridis, K., Vignati, E., Stephanou, E. G., and Wilson, J.: Organic aerosol and
544   global climate modelling: a review, Atmos. Chem. Phys., 5, 1053-1123,
545   https://doi.org/10.5194/acp-5-1053-2005, 2005.
546 Kostenidou, E., Lee, B.-H., Engelhart, G. J., Pierce, J. R., and Pandis, S. N.: Mass Spectra
547   Deconvolution of Low, Medium, and High Volatility Biogenic Secondary Organic
548   Aerosol, Environ. Sci. Technol., 43, 4884-4889, https://doi.org/10.1021/es803676g,
549   2009.
550 Kroll, J. H., Donahue, N. M., Jimenez, J. L., Kessler, S. H., Canagaratna, M. R., Wilson, K.
551   R., Altieri, K. E., Mazzoleni, L. R., Wozniak, A. S., Bluhm, H., Mysak, E. R., Smith,
552   J. D., Kolb, C. E., and Worsnop, D. R.: Carbon oxidation state as a metric for
553   describing the chemistry of atmospheric organic aerosol, Nat. Chem., 3, 133-139,
554   2011.
555 Lee, B. P., Li, Y. J., Yu, J. Z., Louie, P. K. K., and Chan, C. K.: Characteristics of submicron
556   particulate matter at the urban roadside in downtown Hong Kong—Overview of 4

557   months of continuous high-resolution aerosol mass spectrometer measurements, J.
558   Geophys. Res.-Atmos., 120, 2015JD023311, https://doi.org/10.1002/2015JD023311,
559   2015.
560 Lindinger, W., Hansel, A., and Jordan, A.: On-line monitoring of volatile organic compounds
561   at pptv levels by means of proton-transfer-reaction mass spectrometry (PTR-MS)
562   medical applications, food control and environmental research, Int. J. Mass
563   Spectrometry 173, 191-241, http://dx.doi.org/10.1016/S0168-1176(97)00281-4, 1998.
564 Liu, T., Wang, X., Deng, W., Hu, Q., Ding, X., Zhang, Y., He, Q., Zhang, Z., Lü, S., Bi, X.,
565   Chen, J., and Yu, J.: Secondary organic aerosol formation from photochemical aging
566   of light-duty gasoline vehicle exhausts in a smog chamber, Atmos. Chem. Phys., 15,
567   9049-9062, https://doi.org/10.5194/acp-15-9049-2015, 2015.
568 Liu, T., Wang, X., Hu, Q., Deng, W., Zhang, Y., Ding, X., Fu, X., Bernard, F., Zhang, Z., Lü,
569   S., He, Q., Bi, X., Chen, J., Sun, Y., Yu, J., Peng, P., Sheng, G., and Fu, J.: Formation
570   of secondary aerosols from gasoline vehicle exhaust when mixing with SO_2, Atmos.
571   Chem. Phys., 16, 675-689, https://doi.org/10.5194/acp-16-675-2016, 2016.
572 Liu, T., Li, Z., Chan, M., and Chan, C. K.: Formation of secondary organic aerosols from gas-
573   phase emissions of heated cooking oils, Atmos. Chem. Phys., 17, 7333-7344,
574   https://doi.org/10.5194/acp-17-7333-2017, 2017.
575 Liu, T., Wang, Z., Huang, D. D., Wang, X., and Chan, C. K.: Significant Production of
576   Secondary Organic Aerosol from Emissions of Heated Cooking Oils, Environ. Sci.
577   Technol. Lett., 5, 32-37, https://doi.org/10.1021/acs.estlett.7b00530, 2018.
578 Miracolo, M. A., Presto, A. A., Lambe, A. T., Hennigan, C. J., Donahue, N. M., Kroll, J. H.,
579   Worsnop, D. R., and Robinson, A. L.: Photo-Oxidation of Low-Volatility Organics
580   Found in Motor Vehicle Emissions: Production and Chemical Evolution of Organic
581   Aerosol Mass, Environ. Sci. Technol., 44, 1638-1643,
582   https://doi.org/10.1021/es902635c, 2010.
583 Mohr, C., Huffman, J. A., Cubison, M. J., Aiken, A. C., Docherty, K. S., Kimmel, J. R.,
584   Ulbrich, I. M., Hannigan, M., and Jimenez, J. L.: Characterization of Primary Organic
585   Aerosol Emissions from Meat Cooking, Trash Burning, and Motor Vehicles with
586   High-Resolution Aerosol Mass Spectrometry and Comparison with Ambient and
587   Chamber Observations, Environ. Sci. Technol., 43, 2443-2449,
588   https://doi.org/10.1021/es8011518, 2009.
589 Mohr, C., DeCarlo, P. F., Heringa, M. F., Chirico, R., Slowik, J. G., Richter, R., Reche, C.,
590   Alastuey, A., Querol, X., Seco, R., Peñuelas, J., Jiménez, J. L., Crippa, M.,
591   Zimmermann, R., Baltensperger, U., and Prévôt, A. S. H.: Identification and
592   quantification of organic aerosol from cooking and other sources in Barcelona using
593   aerosol mass spectrometer data, Atmos. Chem. Phys., 12, 1649-1665,
594   https://doi.org/10.5194/acp-12-1649-2012, 2012.
595 Nah, T., Kessler, S. H., Daumit, K. E., Kroll, J. H., Leone, S. R., and Wilson, K. R.: OH-
596   initiated oxidation of sub-micron unsaturated fatty acid particles, Phys. Chem. Chem.
597   Phys., 15, 18649-18663, https://doi.org/10.1039/C3CP52655K, 2013.
598 Ng, N. L., Canagaratna, M. R., Zhang, Q., Jimenez, J. L., Tian, J., Ulbrich, I. M., Kroll, J. H.,
599   Docherty, K. S., Chhabra, P. S., Bahreini, R., Murphy, S. M., Seinfeld, J. H.,
600   Hildebrandt, L., Donahue, N. M., DeCarlo, P. F., Lanz, V. A., Prévôt, A. S. H., Dinar,

601   E., Rudich, Y., and Worsnop, D. R.: Organic aerosol components observed in
602   Northern Hemispheric datasets from Aerosol Mass Spectrometry, Atmos. Chem.
603   Phys., 10, 4625-4641, https://doi.org/10.5194/acp-10-4625-2010, 2010.

604 Ng, N. L., Canagaratna, M. R., Jimenez, J. L., Zhang, Q., Ulbrich, I. M., and Worsnop, D. R.:
605   Real-Time Methods for Estimating Organic Component Mass Concentrations from
606   Aerosol Mass Spectrometer Data, Environ. Sci. Techno.l, 45, 910-916,
607   https://doi.org/10.1021/es102951k, 2011a.

608 Ng, N. L., Canagaratna, M. R., Jimenez, J. L., Chhabra, P. S., Seinfeld, J. H., and Worsnop,
609   D. R.: Changes in organic aerosol composition with aging inferred from aerosol mass
610   spectra, Atmos. Chem. Phys., 11, 6465-6474, https://doi.org/10.5194/acp-11-6465-
611   2011, 2011b.

612 Paatero, P., and Tapper, U.: Positive matrix factorization: A non‐negative factor model with
613   optimal utilization of error estimates of data values, Environmetrics, 5, 111-126,
614   https://doi:10.1002/env.3170050203, 1994.

615 Paatero, P.: A weighted non-negative least squares algorithm for three-way 'PARAFAC'
616   factor analysis, Chemometr Intell Lab, 38, 223-242, https://doi.org/10.1016/S0169-
617   7439(97)00031-2, 1997.

618 Presto, A. A., Gordon, T. D., and Robinson, A. L.: Primary to secondary organic aerosol:
619   evolution of organic emissions from mobile combustion sources, Atmos. Chem.
620   Phys., 14, 5015-5036, https://doi.org/10.5194/acp-14-5015-2014, 2014.

621 Qin, Y. M., Tan, H. B., Li, Y. J., Schurman, M. I., Li, F., Canonaco, F., Prévôt, A. S. H., and
622   Chan, C. K.: Impacts of traffic emissions on atmospheric particulate nitrate and
623   organics at a downwind site on the periphery of Guangzhou, China, Atmos. Chem.
624   Phys., 17, 10245-10258, https://doi.org/10.5194/acp-17-10245-2017, 2017.

625 Reyes-Villegas, E., Bannan, T., Le Breton, M., Mehra, A., Priestley, M., Percival, C., Coe,
626   H., and Allan, J. D.: Online Chemical Characterization of Food-Cooking Organic
627   Aerosols: Implications for Source Apportionment, Environ. Sci. Technol., 52, 5308-
628   5318, https://doi.org/10.1021/acs.est.7b06278, 2018.

629 Sage, A. M., Weitkamp, E. A., Robinson, A. L., and Donahue, N. M.: Evolving mass spectra
630   of the oxidized component of organic aerosol: results from aerosol mass spectrometer
631   analyses of aged diesel emissions, Atmos. Chem. Phys., 8, 1139-1152,
632   https://doi.org/10.5194/acp-8-1139-2008, 2008.

633 Struckmeier, C., Drewnick, F., Fachinger, F., Gobbi, G. P., and Borrmann, S.: Atmospheric
634   aerosols in Rome, Italy: sources, dynamics and spatial variations during two seasons,
635   Atmos. Chem. Phys., 16, 15277-15299, https://doi.org/10.5194/acp-16-15277-2016,
636   2016.

637 Sun, Y. L., Zhang, Q., Schwab, J. J., Demerjian, K. L., Chen, W. N., Bae, M. S., Hung, H.
638   M., Hogrefe, O., Frank, B., Rattigan, O. V., and Lin, Y. C.: Characterization of the
639   sources and processes of organic and inorganic aerosols in New York city with a
640   high-resolution time-of-flight aerosol mass apectrometer, Atmos. Chem. Phys., 11,
641   1581-1602, https://doi.org/10.5194/acp-11-1581-2011, 2011.

642 Sun, Y. L., Zhang, Q., Schwab, J. J., Chen, W. N., Bae, M. S., Hung, H. M., Lin, Y. C., Ng,
643   N. L., Jayne, J., Massoli, P., Williams, L. R., and Demerjian, K. L.: Characterization
644   of near-highway submicron aerosols in New York City with a high-resolution aerosol

Atmospheric
Chemistry
and Physics
Discussions

645   mass spectrometer, Atmos. Chem. Phys., 12, 2215-2227, https://doi.org/10.5194/acp-
646   12-2215-2012, 2012.
647 Ulbrich, I. M., Canagaratna, M. R., Zhang, Q., Worsnop, D. R., and Jimenez, J. L.:
648   Interpretation of organic components from Positive Matrix Factorization of aerosol
649   mass spectrometric data, Atmos. Chem. Phys., 9, 2891-2918,
650   https://doi.org/10.5194/acp-9-2891-2009, 2009.
651 United States Department of Agriculture., World vegetable oils supply and distribution,
652   2012/13-2016/17, 2017.
653 Wang, X., Liu, T., Bernard, F., Ding, X., Wen, S., Zhang, Y., Zhang, Z., He, Q., Lü, S., Chen,
654   J., Saunders, S., and Yu, J.: Design and characterization of a smog chamber for
655   studying gas-phase chemical mechanisms and aerosol formation, Atmos. Meas.
656   Tech., 7, 301-313, https://doi.org/10.5194/amt-7-301-2014, 2014.
657 Weitkamp, E. A., Sage, A. M., Pierce, J. R., Donahue, N. M., and Robinson, A. L.: Organic
658   Aerosol Formation from Photochemical Oxidation of Diesel Exhaust in a Smog
659   Chamber, Environ. Sci. Technol., 41, 6969-6975, https://doi.org/10.1021/es070193r,
660   2007.
661 Xu, J., Zhang, Q., Chen, M., Ge, X., Ren, J., and Qin, D.: Chemical composition, sources, and
662   processes of urban aerosols during summertime in northwest China: insights from
663   high-resolution aerosol mass spectrometry, Atmos. Chem. Phys., 14, 12593-12611,
664   https://doi.org/10.5194/acp-14-12593-2014, 2014.
665 Xu, L., Pye, H. O. T., He, J., Chen, Y., Murphy, B. N., and Ng, N. L.: Large Contributions
666   from Biogenic Monoterpenes and Sesquiterpenes to Organic Aerosol in the
667   Southeastern United States, Atmos. Chem. Phys. Discuss., 2018, 1-47,
668   https://doi.org/10.5194/acp-2017-1109, 2018.
669 Zhang, Q., Jimenez, J. L., Canagaratna, M. R., Ulbrich, I. M., Ng, N. L., Worsnop, D. R., and
670   Sun, Y.: Understanding atmospheric organic aerosols via factor analysis of aerosol
671   mass spectrometry: a review, Anal. Bioanal. Chem., 401, 3045-3067,
672   https://doi.org/10.1007/s00216-011-5355-y, 2011.
673 Zhang, X., Cappa, C. D., Jathar, S. H., McVay, R. C., Ensberg, J. J., Kleeman, M. J., and
674   Seinfeld, J. H.: Influence of vapor wall loss in laboratory chambers on yields of
675   secondary organic aerosol, P. Natl. Acad. Sci., 111, 5802-5807,
676   https://doi.org/10.1073/pnas.1404727111, 2014.

Atmospheric
Chemistry
and Physics
Discussions

Open Access

EGU

677   **Table 1.** Experimental conditions in the photochemical aging experiments.

Cooking oil	Dilution ratio	[NMOG]:[NO$_x$] (ppbC:ppb)	OH exposure molec cm^{-3} s	Category	PMF
sunflower	63	4.9	1.0×10^{10}	Pure SOA	NA[a]
olive	107	4.0	1.3×10^{10}	POA+SOA	2 factors
peanut	67	2.6	2.1×10^{10}	Pure SOA	NA
corn	67	3.2	1.8×10^{10}	Pure SOA	NA
canola	67	5.4	3.5×10^{10}	Pure SOA	NA
soybean	67	3.4	1.7×10^{10}	Pure SOA	NA
palm	100	18.9	1.3×10^{10}	POA+SOA	2 factors

678   [a] not applicable.

Atmospheric
Chemistry
and Physics
Discussions

Open Access

679
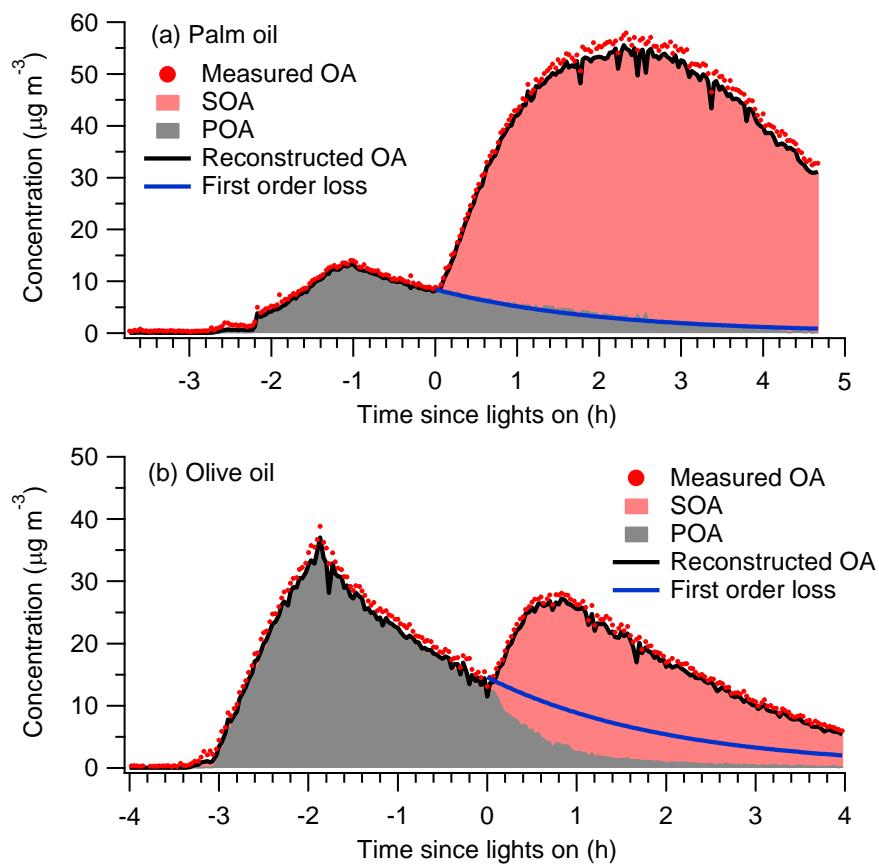
Figure 1. Time series of measured OA, PMF factors, and POA concentrations assuming

681   first-order loss of POA to the walls for (a) palm and (b) olive oil experiments.

682   Concentrations were not corrected for particle wall loss.
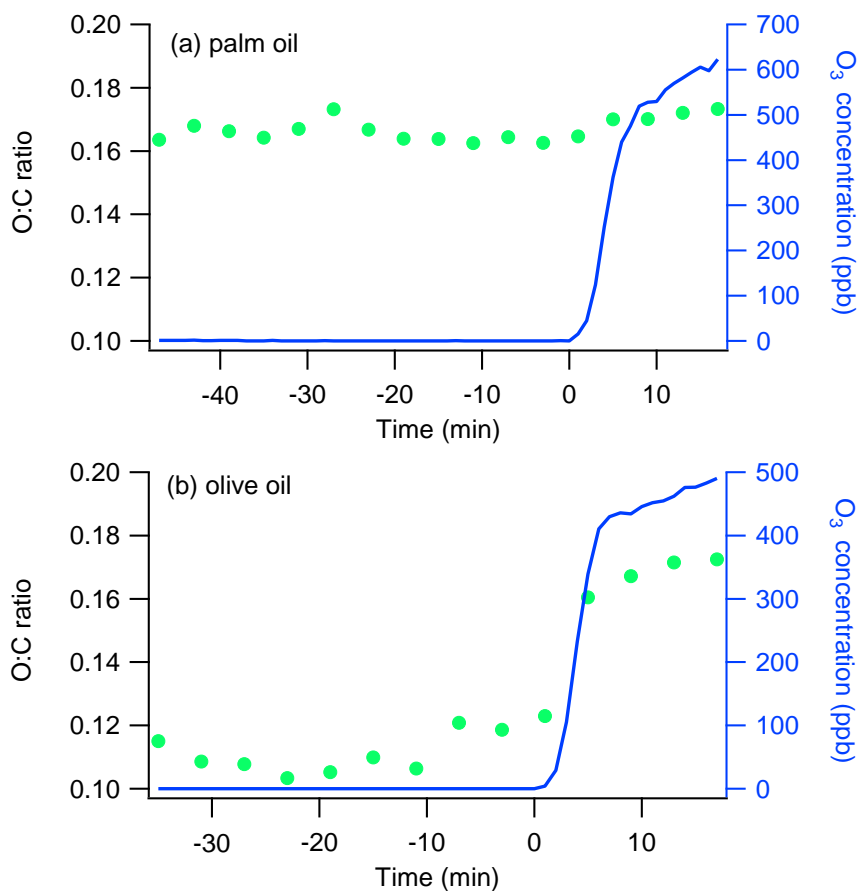
Figure 2. Time series of O:C ratios and O_3 concentrations for oxidation flow reactor

ozonolysis experiments with (a) palm and (b) olive oil. The ozonolysis experiments

involved exposing emissions from palm or olive oil to high concentrations of O_3 in an

oxidation flow reactor. The emissions first passed continuously through the reactor for

at least 30 min and then were exposed to 500–600 ppb ozone for another 17 min. Ozone

was introduced at time $t = 0$.

690
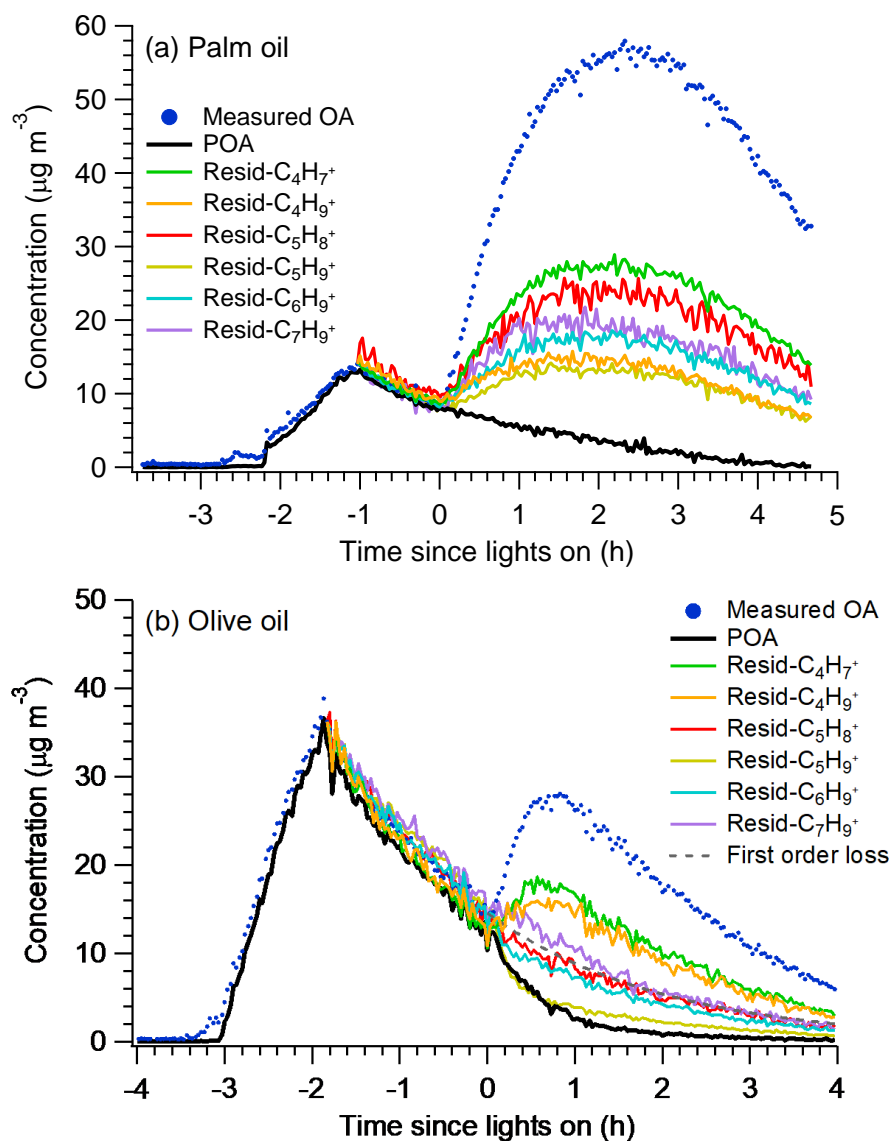
Figure 3. Time series of measured OA, PMF-derived POA factors, and POA

692 determined using the residual method for (a) palm and (b) olive oil experiments.

693

Atmospheric
Chemistry
and Physics
Discussions
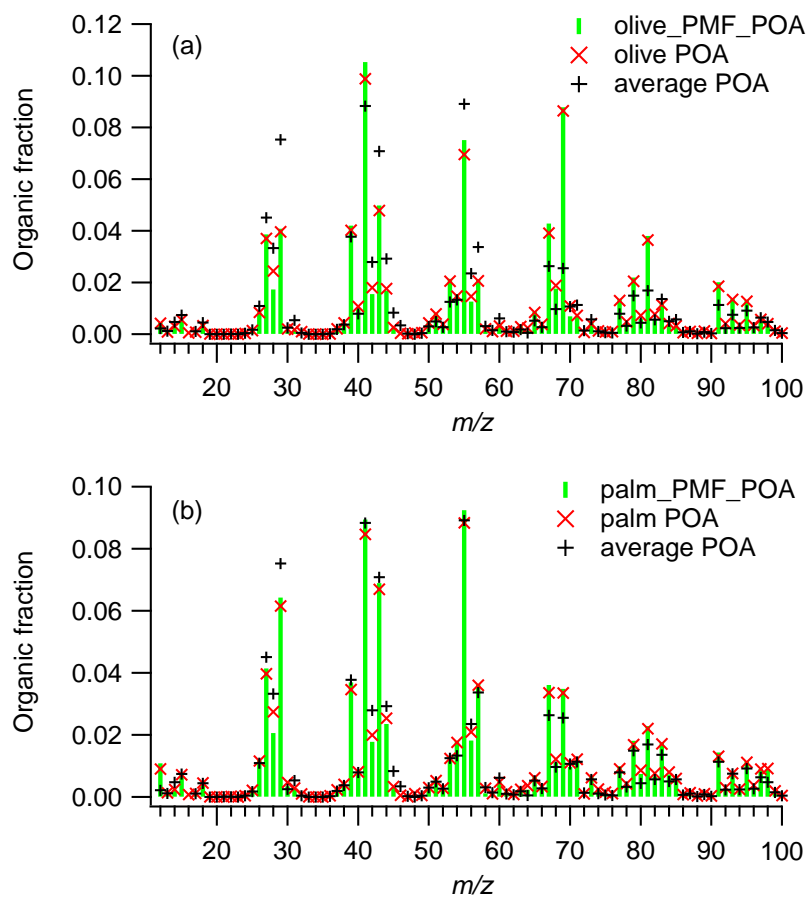
Figure 4. Mass spectra of POA emissions and PMF-derived POA factors for (a) olive

and (b) palm oil and, for comparison, the average mass spectrum of POA emissions

from sunflower, peanut, corn, and canola oils obtained from Liu et al. (2017).

698
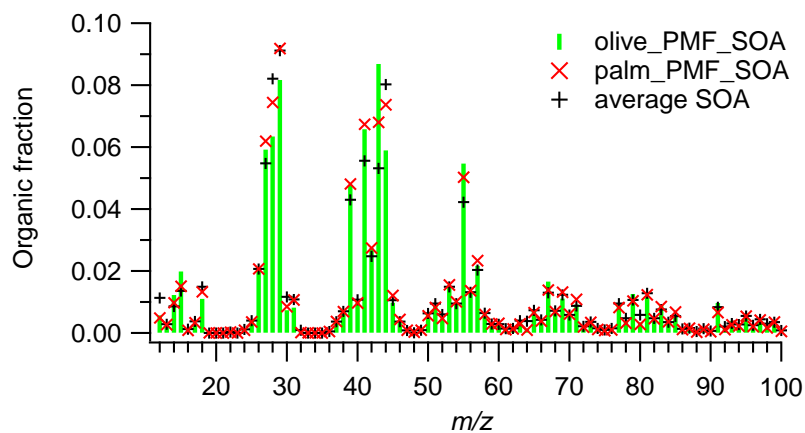
Figure 5. Mass spectra of PMF-derived SOA factors for (a) olive and (b) palm oil and,

for comparison, the average mass spectrum of SOA formed from sunflower, peanut,

corn, canola, and soybean oils. The SOA mass spectra were averaged over a 10 min

period after the OA concentration reached its maximum.
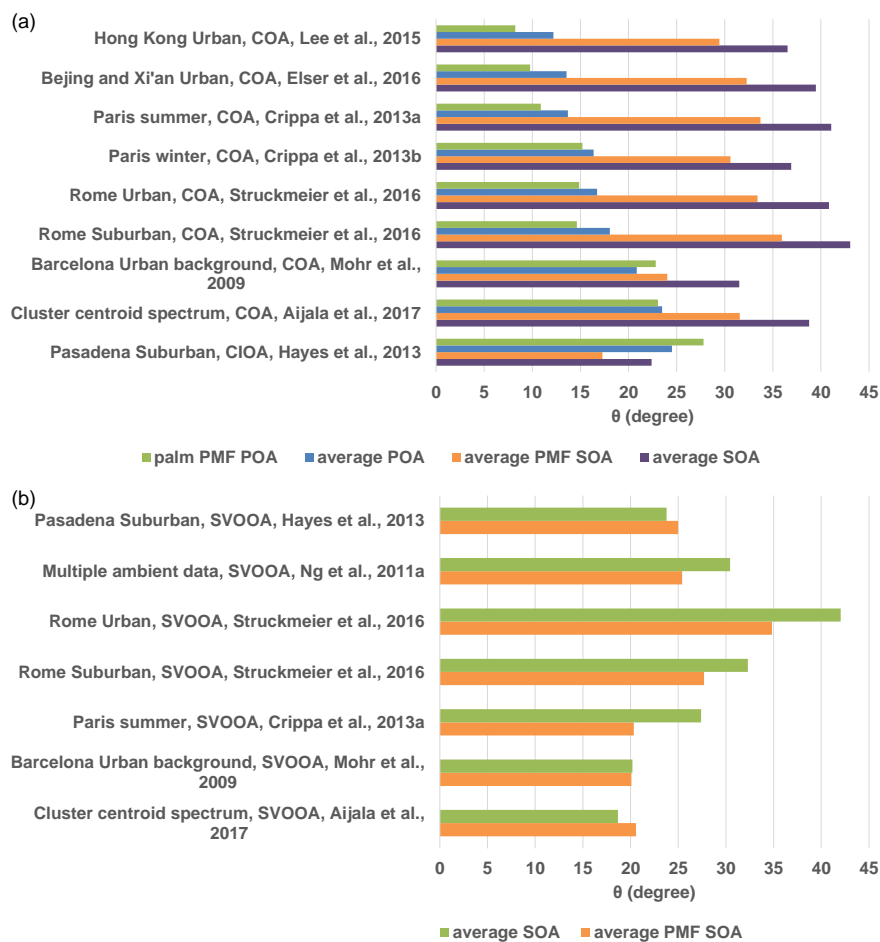
Figure 6. (a) Angles (θ) between ambient COA factor mass spectra and the palm PMF

POA mass spectrum, average POA mass spectrum, average PMF SOA factor mass

spectrum, and average SOA mass spectrum. (b) Angles (θ) between ambient SVOOA

factor mass spectra and the average PMF-derived SOA factor and average SOA mass

spectra. The average POA mass spectra were averaged for sunflower, peanut, corn, and

canola oils (Liu et al., 2017). The average SOA mass spectra were averaged for

sunflower, peanut, corn, canola, and soybean oils in this study.
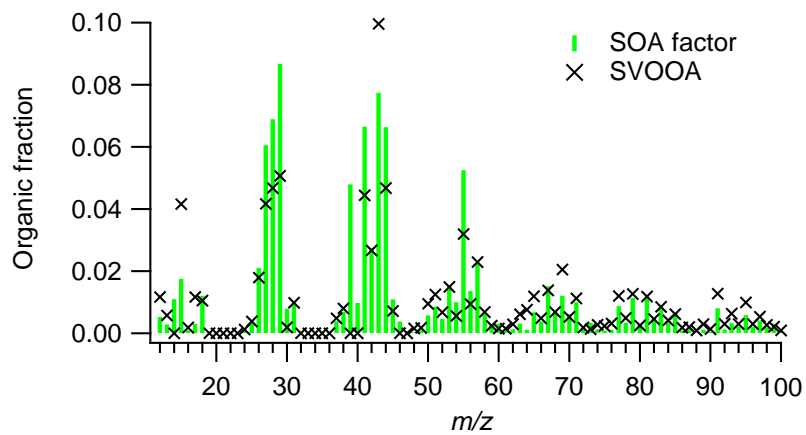
711

712 **Figure 7.** Average PMF SOA factor mass spectrum and ambient SV-OOA factor mass

713 spectrum (Ng et al., 2011a).

Atmospheric
Chemistry
and Physics
Discussions

714

715
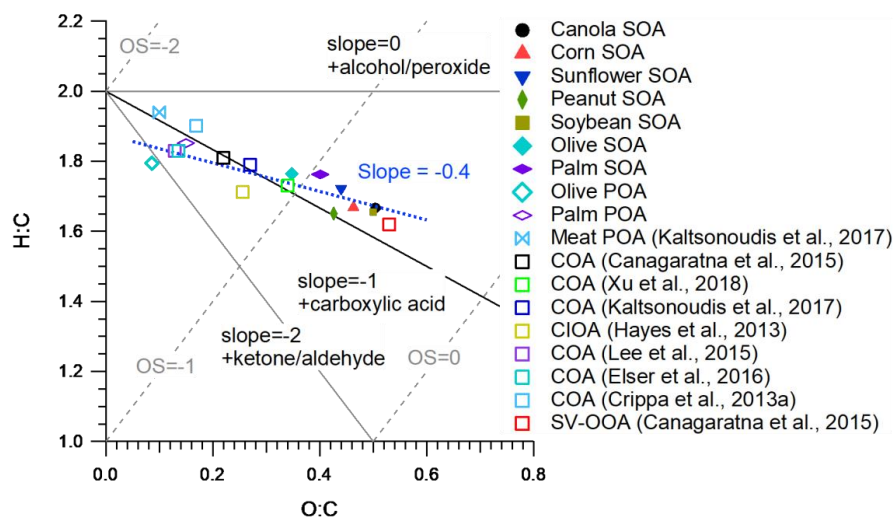
Figure 8. Van Krevelen diagram of POA and SOA from different cooking oils, as well

as ambient PMF factors. Average carbon oxidation states from Kroll et al. (2011) and

functionalization slopes from Heald et al. (2010) are shown for reference.

716

717

718